Table 3. Input parameters for example physical models of 182-413

Stellar spectrum:	$T_* = 39\,000$ K
(Simón-Díaz et al. 2006)	$\log g = 4.1$
	$L_* = 2.04 \times 10^5\ L_\odot$
Ionizing flux at proplyd:	$\Phi_H = 1.27 \times 10^{12}$ cm^{-2} s^{-1}
Ionization front radius:	$r_0 = 3.7 \times 10^{15}$ cm
Gas-phase abundances:	Model A: Esteban et al. (2004)
	Model B: this paper
Dust composition:	Standard Orion (Baldwin et al. 1991)

4 PHOTOEVAPORATION MODELS OF HST 10

We have calculated dynamic photoevaporation models of HST 10, using the procedure outlined in § 6 of Mesa-Delgado et al. (2012). The parameters for the models are shown in Table 3. As compared with 177-341 (HST 1), which was modeled in Mesa-Delgado et al. (2012), HST 10 receives a roughly ten times smaller ionizing flux and is roughly twice as large. Since $F \propto n^2 r$ for recombination-dominated photoevaporation flows (Bertoldi & McKee 1990; Henney 2001), this implies that the densities in HST 10 should be $\simeq 5$ times smaller and the ionization parameter $\simeq 2$ times smaller than in HST 1.

Two different abundance sets were used in the models. The first (Model A) is the standard Orion gas phase abundance set, as determined by Esteban et al. (2004). The second (Model B) is the set of abundances determined in this paper by empirical means, see Table 3. The resultant spectrum is shown in Figure 8 for the two cases. It can be seen that the Esteban et al. abundances produce very large discrepancies between the observed and predicted line fluxes (panel a). In particular, all Sulfur, Argon and Chlorine lines are too strong in the model by a factor of 3 to 10, whereas, [O III] 4363 Å is too weak, indicating that the model temperature is too low in the highly ionized regions. On the other hand, the [N II] lines are well-reproduced y this model.

The situation is much improved by using the Model B abundances (panel b), although serious discrepancies remain. The sulfur line fluxes are now in good agreement with the observations, with the notable exception of the [S II] 4070 Å auroral line, which is still 3 times too strong in the model. The [O I] 6300 Å shows a similar behaviour, being too strong by a factor of 4. These two lines, together with the [N II] 5755 Å auroral line, show the strongest contrast between the proplyd and the background nebula, and hence are measured with a relatively small uncertainty, making the disagreement highly significant. The [N II] lines do not agree with Model B so well as they do with Model A, but the agreement is still fair given the uncertainties. The remaining disagreement is with the [N I] 5199 Å line, but this is to be expected since the line arises through fluorescence in neutral gas (Ferland et al. 2012), whereas the model extends only to a hydrogen ionization fraction of 0.1 and therefore misses part of the [N I]-emitting zone.

It is not particularly surprising that the empirically determined abundances do not reproduce the observed fluxes when used in our physical proplyd model. The same was seen in the case of HST 1, where it was argued that the strong gradients in temperature and density, both with and between ionization zones, invalidated the empirical one-zone or two-zone approaches for analysing the spectrum. However, in that case it was possible to find a different set of abundances for the model that succeded in reproducing the observed spectrum to a high precision. Unfortunately, we have been unable to find such a satisfactory model for HST 10. Initial attempts to adjust the abundances have resulted in models that fit the observations *worse* than Model B does.

The two most discrepant lines, [O I] 6300 Å and [S II] 4070 Å have a considerable overlap in their zones of emission. All the [O I] emission, and roughly half of the [S II] 4070 Å arises from partially ionizes gas at the ionization front itself. If the temperature of this gas is overestimated in the models, then the discrepancy could be explained. With the standard Orion dust properties that we are using in all the models (Baldwin et al. 1991), photoelectric emission from dust grains provides up to 15% of the heating in this zone. Since there is some evidence that dust is depleted in the proplyd flows (García-Arredondo et al. 2001), it may be feasible to reduce this heating, which is an avenue that will be explored in future work.

REFERENCES

Baldwin J. A., Ferland G. J., Martin P. G., Corbin M. R., Cota S. A., Peterson B. M., Slettebak A., 1991, ApJ, 374, 580

Bertoldi F., McKee C. F., 1990, ApJ, 354, 529

Esteban C., Peimbert M., García-Rojas J., Ruiz M. T., Peimbert A., Rodríguez M., 2004, MNRAS, 355, 229

Ferland G. J., Henney W. J., O'Dell C. R., Porter R. L., van Hoof P. A. M., Williams R. J. R., 2012, ApJ, 757, 79

García-Arredondo F., Henney W. J., Arthur S. J., 2001, ApJ, 561, 830

Henney W. J., 2001, in Revista Mexicana de Astronomia y Astrofisica Conference Series, Vol. 10, Revista Mexicana de Astronomia y Astrofisica Conference Series, Cantó J., Rodríguez L. F., eds., pp. 57–60

Mesa-Delgado A., Núñez-Díaz M., Esteban C., García-Rojas J., Flores-Fajardo N., López-Martín L., Tsamis Y. G., Henney W. J., 2012, ArXiv e-prints

Simón-Díaz S., Herrero A., Esteban C., Najarro F., 2006, A&A, 448, 351

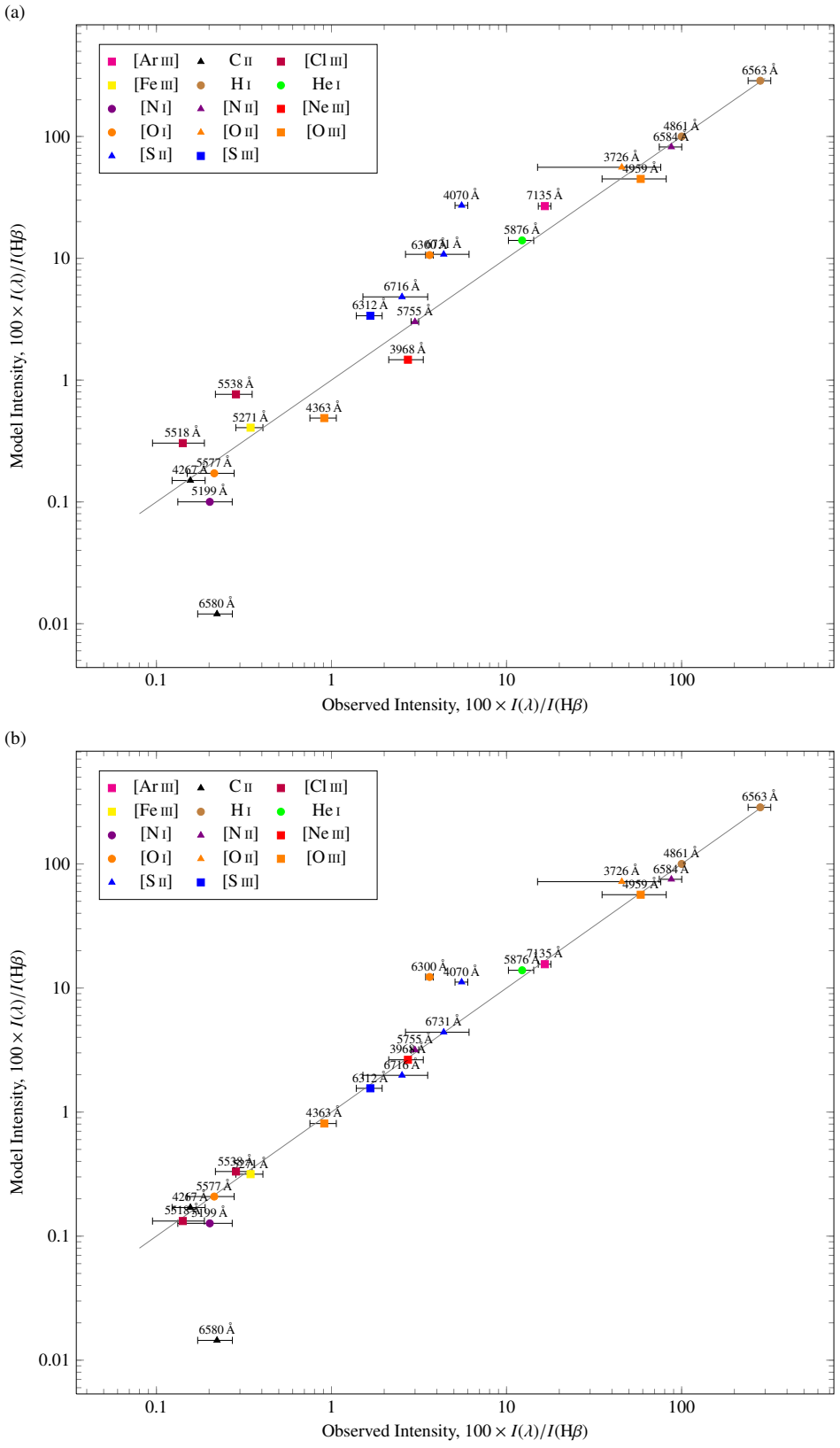

Figure 8. Comparison between predicted and observed emission line fluxes for photoevaporation models of HST 10 with (a) abundances as determined for the Orion Nebula by Esteban et al. (2004), (b) abundances determined for HST 10 in this paper. The agreement in panel (b) is much better, but there are still notable discrepancies.

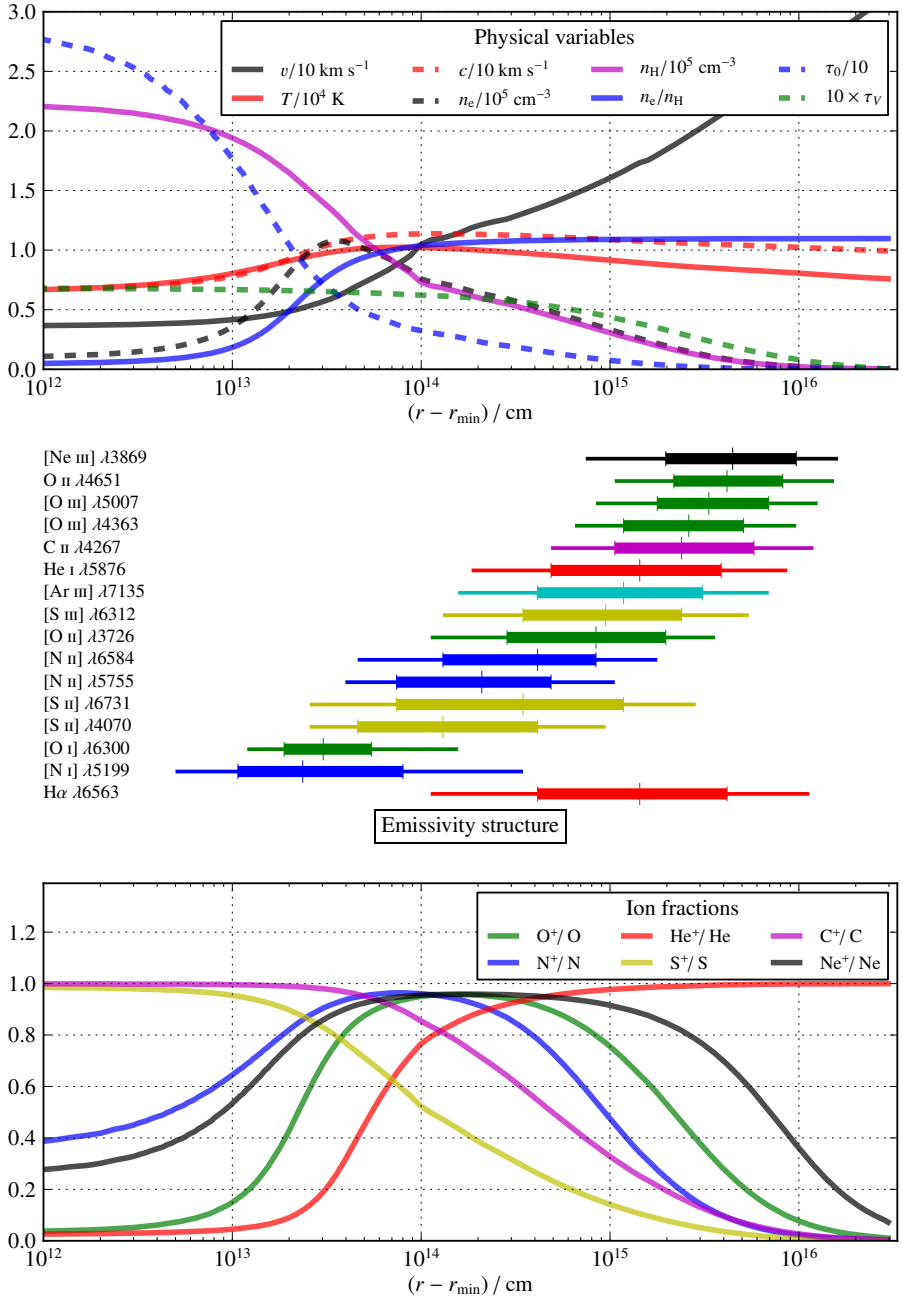

Figure 9. Model structure as a function of radius along a line at an angle of $\theta = 30°$ to the symmetry axis for our photoevaporation Model B. The radius r is measured from the center of curvature of the ionization front, shown on a logarithmic scale with respect to the deepest point in the model, $r_{\rm min} = 3.5 \times 10^{15}$ cm. *Upper panel*: Physical variables. Gas velocity, v, in units of 10 km s^{-1} (solid black line). Gas temperature, T, in units of 10^4 K (solid red line). Isothermal sound speed, c, in units of 10 km s^{-1} (dashed red line). Electron density, $n_{\rm e}$, in units of 7×10^4 cm^{-3} (dashed black line). Total hydrogen density, $n_{\rm H}$, in units of 7×10^4 cm^{-3} (solid purple line). Electron fraction, $n_{\rm e}/n_{\rm H}$ (solid blue line). Lyman limit optical depth, τ_0 (divided by 10), measured from the ionizing source, which is located off the graph at $r = 6.32 \times 10^{17}$ cm (dashed blue line). Visual dust extinction optical depth, τ_V (times 10). *Middle panel*: Emissivity structure for selected emission lines. For each emission line, the vertical line indicates the median emission radius (for which half the total line flux is emitted from gas at smaller radii and half from gas at larger radii), while the thick horizontal bar shows the range between the 25th and 75th quartiles of the emission, and the thin horizontal bar shows the range between the 10th and 90th quartiles of the emission. *Lower panel*: Ionization structure. The fraction of singly ionized ions for a selection of elements is shown by differently colored lines, as indicated in the key. Results for other angles and abundance sets are similar, except with densities that scale roughly as $\cos^{1/2}\theta$, and temperatures that tend to decrease slightly with θ and with increased metal abundances.